Supplementary Notes

In this Supplementary Information, we give more details about the Via Lactea II (VL-II) simulation presented in our Letter. The first part provides additional results about radial trends in subhalo abundance and properties. In the second part we include some comparisons with the Via Lactea (VL-I) run, previously the largest simulation of the Galactic dark matter halo.

Supplementary Figure 1 illustrates how tidal interactions with the gravitational potential of the host shape the radial distribution of subhalos and their internal structure. Tides remove mass from the outer parts of subhalos. Clumps closer to the Galactic center lose more mass as they experience stronger tidal forces and more pericenter passages[18]. Mass loss also reduces $V_{\rm max}$ and $r_{\rm Vmax}$, which leads to an increase in $\bar{\rho}(< r_{\rm Vmax})$. The radial distribution of subhalos with $V_{\rm max} > 3\,{\rm km\,s^{-1}}$ is more extended than the dark matter distribution in the Galactic halo, a feature that does not depend on subhalo size, i.e. different $V_{\rm max}$ selection thresholds lead to the same radial distribution. VL-II resolves subhalos as close as 8 kpc from the Galactic center, but it is possible that it underestimates the true substructure abundance inside 20 kpc due to numerical limitations. Subhalo concentrations are defined as the mean density within $r_{\rm Vmax}$, the radius of peak circular velocity, a quantity that is well determined both for isolated halos and subhalos and does not dependent on assumptions about their density profiles[18]:

$$c_V \equiv \bar{\rho}(< r_{\rm Vmax})/\rho_{\rm crit,0} = \left(V_{\rm max}/r_{\rm Vmax}\right)^2 4\pi/(3G\rho_{\rm crit,0}), \qquad (1)$$

where $\rho_{\rm crit,0} = 1.48 \times 10^{-7}\ {\rm M_\odot\,pc^{-3}}$. The median subhalo concentration increases strongly towards the Galactic center, both because of tidal mass losses and to a lesser extent because of the earlier formation times of inner substructure[18].

Supplementary Table 1 summarises the numerical parameters and host halo properties of the VL-I and VL-II simulations. The main difference between these runs is the improved time stepping in VL-II, which at each time and for each particle is based on the local dynamical time $\sqrt{1/G\rho_{\rm enc}}$[19], where $\rho_{\rm enc}$ is the mean density enclosed in a sphere extending out to the particle's position and centered on the dynamically dominant structure. In VL-I we adopted instead the standard ad-hoc time-step criterion based on the acceleration and the gravitational softening of the particle ($\propto \sqrt{\epsilon/|\mathbf{a}|}$). This criterion fails in high density regions and artificially flattens the inner cuspy halo density profiles[31]. This limitation set the convergence radius of VL-I (where the host true density profile is reproduced to within 10 percent) to $r_{\rm conv} = 1.3$ kpc. The new time stepping used in VL-II allows us to properly resolve the host density profile on significantly smaller scales: the finite mass resolution determines a convergence radius[20] of about 0.38 kpc for VL-II. The VL-I subhalo density profiles are also affected by this limitation: the enclosed densities within 300 pc of large subhalos are about twice as high in VL-II. Further out, at 600 pc, the enclosed subhalo densities are very similar in VL-I and VL-II.

To check for numerical convergence and test the dependence of our results on numerical and cosmological parameters we ran a series of lower resolution versions of VL-II. The mass resolution in this "VL-IIm" series is 64 times coarser and the force softening length 4 times larger than in VL-II. Supplementary Figure 2 shows that the lower resolution version of the same halo has a very similar subhalo velocity function above about $0.05\,V_{\rm max,host} \simeq 10\,{\rm km\,s^{-1}}$. Rescaling to 64 times less massive systems suggests that VL-II should have converged down to about 2.5 $\rm km\,s^{-1}$, which indeed is close to the scale where the VL-II velocity function starts to fall below the power law fit (Figure 3). The earlier starting redshift of VL-II does not seem to affect the $z = 0$ substructure abundance significantly. We find only a weak dependence on cosmological parameters: VL-II used the best fit ΛCDM parameters from the *WMAP* 3 year data release[14]: $\Omega_m = 0.238$, $\Omega_\Lambda = 0.762$, h=0.73, n_s=0.951, and σ_8=0.74. For comparison we have ran a simulation with *WMAP* 1 year parameters[32]: $\Omega_m = 0.27$, $\Omega_\Lambda = 0.73$, h=0.72, n_s=1.0, and σ_8=0.9. The higher σ_8 and steeper spectral index n_s in *WMAP1* lead to more small scale power. The effect on the $z = 0$ substructure abundance is rather small: our WMAP1 run has about 20 to 30 percent more subhalos relative to the WMAP3 runs, in agreement with semi-analytical predictions (see Figure 11 in[33]).

31. Diemand, J., Zemp, M., Stadel, J., Moore, B. & Carollo, C. M. Cusps in cold dark matter haloes. Mon. Not. R. Astron. Soc. 364, 665–673 (2005).

32. Spergel, D. N. et al. First-Year Wilkinson Microwave Anisotropy Probe (WMAP) Observations: Determination of Cosmological Parameters. Astrophys. J. Supp. 148, 175–194 (2003).

33. Zentner, A. R. & Bullock, J. S. Halo Substructure and the Power Spectrum. Astrophys. J. 598, 49–72 (2003).

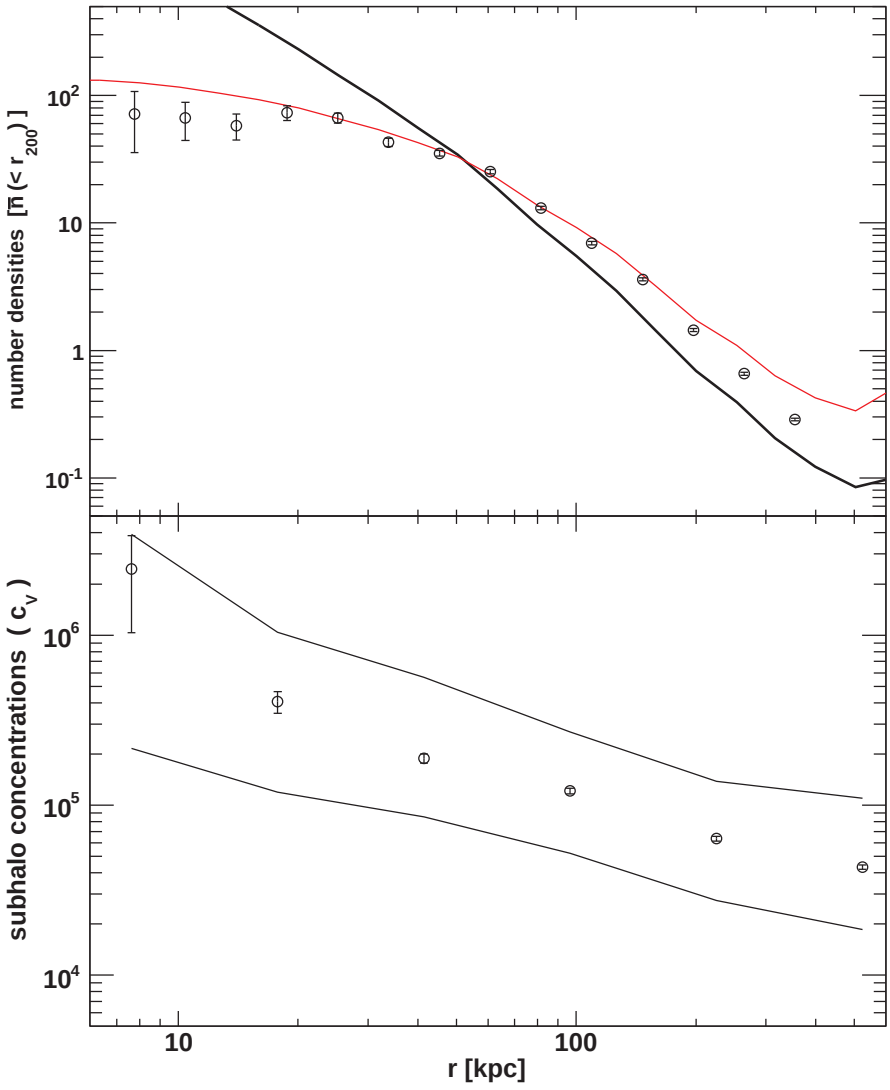

Supplementary Figure 1: Abundance and concentrations of subhalos vs. distance from the galactic center. *Top:* The number density profile of subhalos (circles) is more extended than the dark matter density profile $\rho(r)$ (thick line). Their ratio turns out to be roughly proportional to the enclosed mass $M(< r)$, i.e. $\rho M(< r)$ (thin line) matches the subhalo number density quite well. Only subhalos larger than $V_{\rm max} = 3\,{\rm km\,s^{-1}}$ are included here. *Bottom:* Subhalo concentrations (median and 68% range are shown) increase towards the center, where the stronger tidal force remove more of the outer, low density parts from the subhalos. To make sure their c_V are resolved, only subhalos larger than $V_{\rm max} = 5\,{\rm km\,s^{-1}}$ are used. The error bars indicate the statistical uncertainties in both panels.

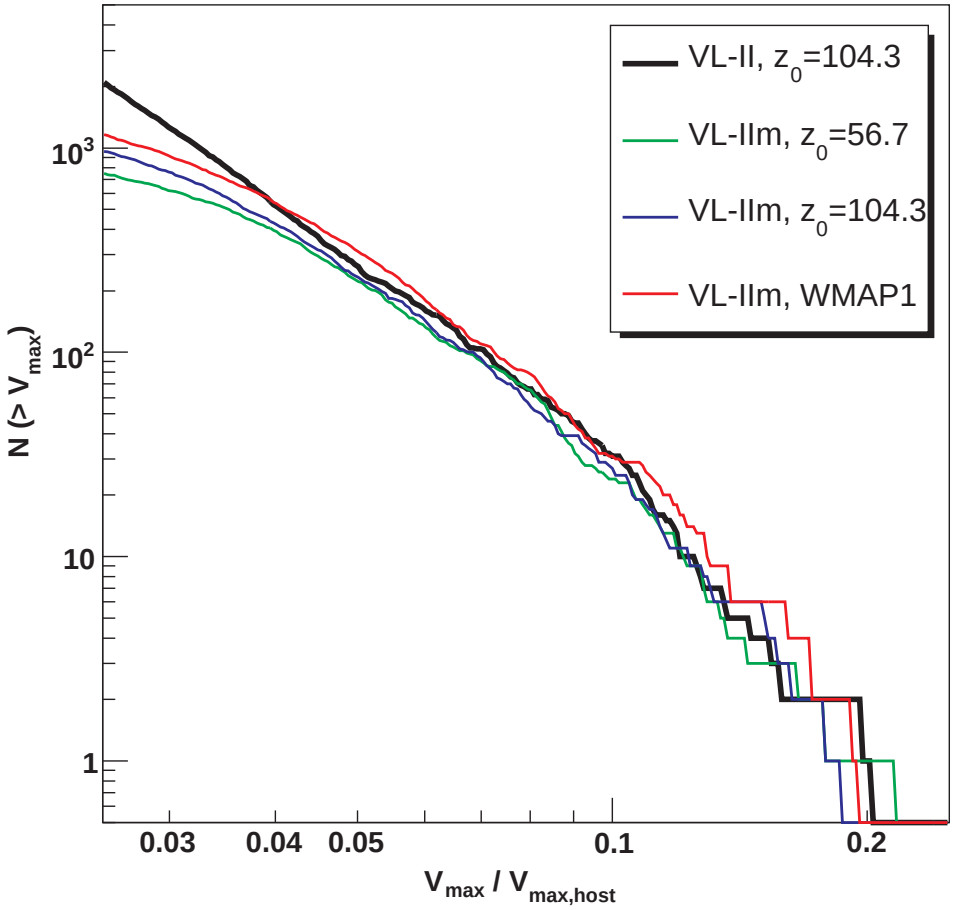

Supplementary Figure 2: Subhalo abundance at different numerical resolutions, starting redshifts and cosmologies. Number of subhalos above $V_{\rm max}/V_{\rm max,host}$ within r_{200} for the VL-II simulation and three lower resolution versions of the same halo.

Name	ΔT	ϵ (pc)	z_i	$r_{\rm conv}$ (kpc)	$M_{\rm hires}$ ($M_\odot$)	r_{200} (kpc)	M_{200} ($M_\odot$)	$V_{\rm max}$ (km s^{-1})	$r_{\rm Vmax}$ (kpc)
VL-I	$0.2\sqrt{\epsilon/\lvert\mathbf{a}\rvert}$	90.0	48.4	1.3	2.1×10^4	389	1.77×10^{12}	181	69
VL-II	$0.06\sqrt{1/G\rho_{\rm enc}}$	40.0	104.3	0.38	4.1×10^3	402	1.93×10^{12}	201	60

Supplementary Table 1: Simulation parameters and halo properties. Time step criterion ΔT, spline force softening length ϵ, initial redshift z_i, convergence radius of the host halo density profile $r_{\rm conv}$, mass $M_{\rm hires}$ of high resolution dark matter particles and host halo r_{200}, M_{200}, $V_{\rm max}$ and $r_{\rm Vmax}$ for the VL-I and VL-II simulations. At each time individual particle time steps are chosen by dividing the base time step of 13.7 Gyr / 400 by two until it is smaller than ΔT, where $|a|$ is the norm of the acceleration vector and $\rho_{\rm enc}$ is the enclosed density within the dynamically dominant structure. Force softening lengths ϵ are constant in physical units back to $z = 9$ and constant in comoving units before.